24th COBEM - 2017

ABCM 24th International Congress of Mechanical Engineering
December 3-8, 2017, Curitiba, Brazil

COBEM-2017-1350
THERMO-PHYSICAL ANALYSIS OF THE CHARACTERISTICS OF AL-FE-ZR-(1,8; 5,0)WT%MG ALLOYS SOLIDIFIED IN HORIZONTAL UNIDIRECTIONAL MOLD

Yan Araujo Santos da Campo
Universidade Federal de Santa Maria (UFSM), Santa Maria/Rio Grande do Sul/Brasil.
yanaraujosantos@gmail.com
Marcus Vinícius Wanderley
Rafael Assis da Silva
Mauro Quaresma Lobato
José Maria do Vale Quaresma
Universidade Federal do Pará (UFPA), Belém/Pará/Brasil.

Abstract. *The Al-Mg alloys constitute an important group of aluminum alloys. Beyond of mechanical resistance gains, the magnesium allows keep excellent corrosion resistance and weldability. This paper aims to analyze Al-0,12wt%Fe-0,20wt%Zr-1,8wt%Mg and Al-0,12wt%Fe-0,20wt%Zr-5,0wt%Mg alloys. For the solidification a horizontal unidirectional mold was used in the form of a cubic chamber with six faces containing a single metallic face. In this way, the thermal performance can be evaluated: as solidification rate and cooling rate, besides macro-structural behavior and solute rejection, correlating it with microhardness. In the results, the alloy with 5,0wt% Mg presented higher solidification rate from the 15,0 mm position. The alloy with 1,8wt% Mg presented higher cooling rate in the initial positions. The increase in magnesium composition caused a decrease in grain size. The results of microhardness followed the behavior of solute rejection of magnesium.*

Keywords: *Al-Mg alloys, solidification, speed and rate of solidification, solute rejection, thermos-physical analysis.*

1. INTRODUCTION

Aluminum is historically of significant importance within the materials science, and has played a crucial role in the metallurgical and mechanical industry. For Davis (1993) some characteristics of aluminum alloys are light weight, electrical and thermal conductivity, water resistance, high ratio of strength/weight ratio, excellent aesthetic appearance, durability, formability, corrosion resistance, hardness, diversity of aesthetic finishes and recyclability. This work thermos-physical address the behavior of Al-0,12wt%Fe-0,20wt%Zr-1,8wt%Mg alloy and Al-0,12wt%Fe-0,20wt%Zr-5,0wt%Mg unidirectional solidified in the mold of the horizontal cubic type of ceramic fiber subsequent objectives and will evaluate, based on the rate of solidification speed and to evaluate their behavior and macrostructural solute distributions from the metal/mold interface. For this, they will be used in addition to theoretical procedures, experimental procedures performed in the mechanical engineering laboratory of the Federal University of Pará (UFPA). The work was proposed from studies by Research Group on Materials Engineering (GPEMAT) which has as one objective to analyze and study the thermos-physical and mechanical properties of aluminum alloys and characterize them as their thermal behavior when solidification, after solidification mechanical; and the works which have unique characteristics of aluminum alloys with varying addition of Mg, as Robinson's (2007a).

2. GENERAL OBJECTIVES

This work has as main objective to analyze the thermos-physical performance of unidirectionally solidified Al-0,12wt%Fe-0,20wt%Zr-1,8wt%Mg and Al-0,12wt%Fe-0,20wt%Zr-5,0wt%Mg alloys in cubic refractory fiber mold with a single metallic interface of steel 1010, a model used in studies of the work of Quaresma (1999) on solidification thermal performance for Al-Cu and Al-Cu-Fe (commercial) alloys.

Subsidizing the main objective will be evaluated the following parameters for both alloys:

- Solidification curves;
- Solidification speeds;

- Solidification rates;
- Macrographs of the alloys;
- Microhardness of the alloys.

3. LITERATURE REVIEW

3.1 Alloying elements

For Garcia (2001a), the additions of alloying elements are important in casting alloys due to improvement of its characteristics, such as increased flow and reduced brittleness at hot and also due to improvement of corrosion resistance, machinability and weldability. The search for property improvements culminated in the development of numerous alloys with many different combinations of elements. The alloy elements used in the study will be discussed below:

According to the HANDBOOK OF ALUMINUM (2013a), virtually all the aluminum alloys contain some amount of iron (Fe) which is an impurity remaining from bauxite refining and casting. The phase diagram [...] provides that during solidification of an Fe-Al alloy containing a few tenths of iron, most of this remains in the liquid phase to a solid eutectic solution more intermetallic constituent particle with a Al_3Fe monoclinic solidified crystalline structure. Depending on the rate of solidification and the presence of other elements, such as Mn, may form constituent particles of Al_6Fe phase orthogonal metastable rather than equilibrium Al_3Fe. The maximum solubility of iron in solid aluminum is 0,05%.

The addition of zirconium (Zr) affords the precipitation of Al_3Zr *dispersoids*, which may not provide significant enhancement scatter (due to their low volume fraction). However, Al_3Zr *dispersoids* to prevent recrystallization, and therefore give extensive reinforcement to limit the grains to small grains (HANDBOOK OF ALUMINUM, 2013b).

Magnesium (Mg) provides substantial improvement in strengthening and hardening characteristics of the mechanical working of aluminum. It has a relatively high solubility in solid aluminum but Al-Mg alloys containing less than 7wt% Mg does not exhibit appreciable characteristics of heat treatment. Magnesium is also added in combination with other elements, notably copper and zinc, for even greater improvements in strength (HANDBOOK OF ALUMINUM, 2013c).

For Chiaverini (1977), the addition of elements become an integral part of the solid phase, the resulting layer is called "solid solution"; this therefore the pure metal dissolves intentionally added element.

3.2 Solidification

Solidification became science from the last sixty years, which allowed a better understanding of heterogeneities, causes and effects, indicating control parameters, subject to change, enabling foundry processes optimized and maximized end products in terms of quality and final performance. The solidification takes place in two successive stages of nucleation and growth. Nucleation reflects the way in which the solid phase appears stably within the liquid phase growth and reflects the way in which these nuclei grow (Kurz and Fisher, 1992).

According to Garcia (2001b), some thermal parameters are essential in the study of solidification, such as local solidification time, growth rates, temperature gradients and solidification (or cooling) rates. These are presented below.

3.2.1 Local time of solidification

It is defined as the difference between the transit time of the *solidus isotherm* (T_{Sol}) and the transit time of the *liquidus isotherm* (T_{Liq}) for a given point on the workpiece solidification as illustrated below:

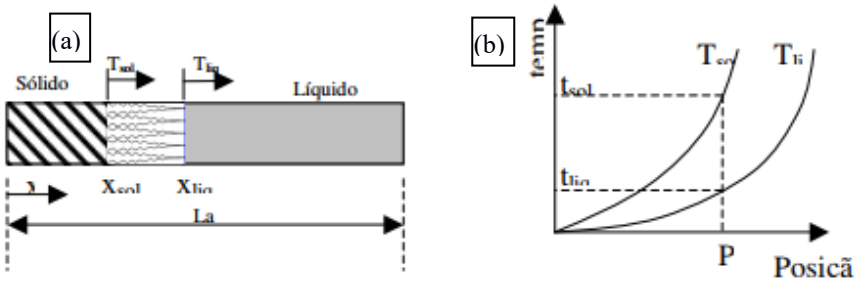

Figure 1. Illustration of the evolution of T_{Liq} by position (a) and graphic of evolution of the *isotherm*s (b) during solidification (adapted from Souza, 2004)

3.2.2 Solidification speed

The solidification rate is defined as the distance between two consecutive points T_{Liq} (ΔX) at time intervals it took to cover this distance. Thus obtained T_{Liq} the feed rate, as illustrated below:

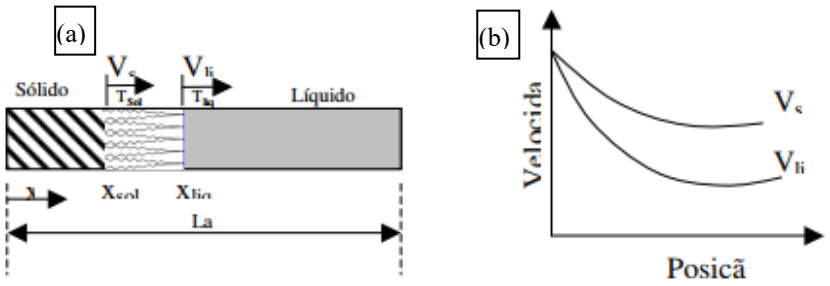

Figure 2. Illustration of the displacement T_{Liq} (a) and graphic of evolution of the speed of advance of the *isotherm*s as a function of position (b) during solidification (adapted from Souza, 2004)

3.2.3 Solidification rate

The cooling rate ($\dot{T}$) is defined by the slope of the cooling curve when passing through the *liquidus* temperature is understood to be:

$$\dot{T} = \frac{\partial T_{liq}}{\partial t} \tag{1}$$

3.2.4 Macrostructure of solidification

According to Rodrigues (2007b), the macrostructure of solidification can present three separate areas, as shown in Figure 4:

- A known *chill* (or *shell*) zone characterized by small grains produced by rapid heat extraction along the metal/substrate interface, predominantly nucleation growth;
- An elongate zone in the direction of heat extraction, comprising fine crystals called *columnar*, characterized by extending to the front zone *chilled*;
- A random disordered region growing crystals, *equiaxed* denominated in the center of the melt.

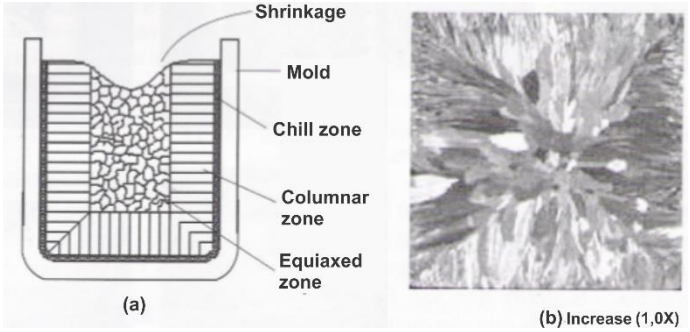

Figure 3. Schematic representation of the different zones macrostructural (a); (b) macrostructure of a square section aluminum sample (adapted from Garcia, 2001)

The solidification macrostructure is dependent on various factors such as overheating of the liquid, chemical composition, fluid flow, the addition of grain refiners and size of the melt, for example.

4. MATERIALS AND METHODS

4.1 Equipment used

The alloys developed for analysis in this study were obtained by direct casting from an aluminum base with additions of Zr and Mg solutes. After weighing the aluminum and other elements used in this work, the mass of materials was introduced into a 3,5 L silicon carbide crucible, which is internally painted with kaolin solution to prevent the adhesion of metals with their Interior walls.

The melting of metals was carried out in a muffle furnace, Figure 5 (a), the Brasimet mark. After verified the complete fusion of the metal, around 900° C, the crucible is removed from the oven, Figure 5 (b), and then is held homogenization of molten metal, Figure 5 (c), by vigorous stirring with a spatula steel. Thus, homogenization done made to inject inert gas (argon), Figure 5 (d), at a flow rate between 0.2 and 0,4 L/s through a stainless-steel tube connected to a cylinder 10m³ introduced into the hole in insulator placed on a refractory crucible. This is done to remove gases and low density impurities, a slag forming the surface layer removed by the spatula to be after performing the casting process the material.

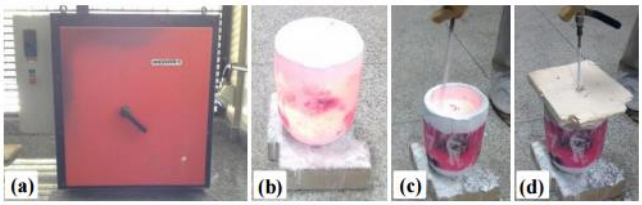

Figure 4. (a) a muffle furnace, (b) crucible containing the molten metal, (c) homogenization using a steel spatula, (d) injecting argon gas for removal of impurities with low density (GPEMAT, 2016).

After the above process, there was leakage of material removal of the control sample, made of a steel mold which is prepared by following procedures: sanding and painting with heating kaolin solution. After removing the specimen for chemical analysis (control sample), a thermocouple was introduced into the crucible in order to verify metal temperature, until it reaches the temperature value set for the completion of the leak. Achieving this temperature, leakage was held a horizontal unidirectional mold, based on this work Quaresma (1999).

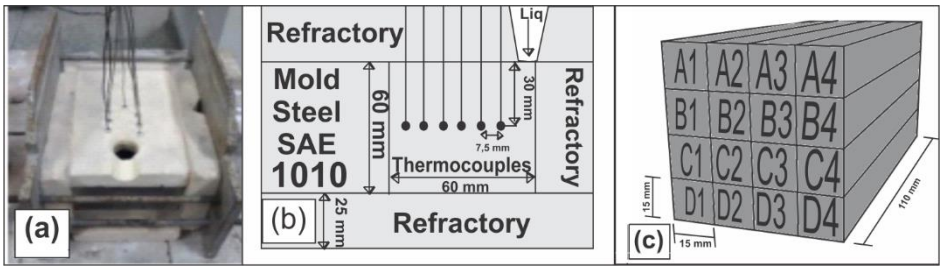

Figure 5. (a) front view with the mold thermocouples, (b) mold template with thermocouples positions, (c) ingot template obtained after casting. (GPEMAT, 2016)

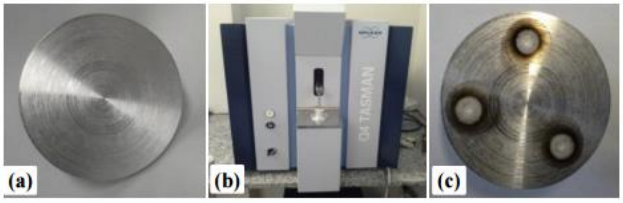

Figure 6. Witness sample (a), mass spectrometer (b) and (c) sample after the chemical analysis (GPEMAT, 2016)

By measuring the control sample approximately 501 mm in diameter, Figure 7 (a), was held on the chemical analysis by the mass spectrometer, Figure 7 (b), where the results are obtained from the average of at least three readings the chemical composition of the sample, Figure 7 (c).

After the undercut, the obtained sections were labeled with dimensions [15x15x110] mm and cut with the aid of a saw.

Samples underwent a grinding and polishing process. The p rocedures used for these assays are consistent with the normative standard ASTM E384. For calculating the average of each distance on the metal/mold interface, 45

measurements were used for each sample. Measurements were performed on three lines on each piece 15 measurements on each line.

The analysis of microhardness they were performed in a HV-1000B equipment according to Figure 8. Test loads of 0,98N were used and a pyramid indenter with a regular basis vertex 136º, to determine the Vickers hardness of the material were used.

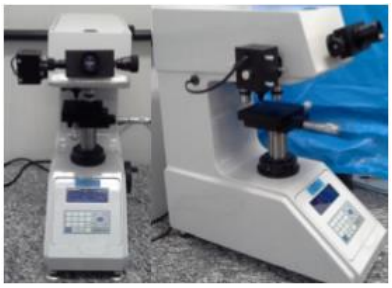

Figure 7. Microdurometer HV-1000B (GPEMAT, 2014)

4.2 Determination of the solidification parameters

To obtain the solidification parameters (V_L and $\dot{T}$) the following experimental and analytical procedures were performed:

- Graphics obtaining time-temperature profiles for each position during solidification (data acquired by thermocouples distributed in equal distances from the metal interface, as shown in the previous section);
- Determining T_L passage time obtained for each position and the position versus time graph, generating function P(t) (position) *versus* T (time). The derivative (in time) of this function will set the solidification rate versus time. Using numerical properties logarithms are obtained from the equation of velocity *versus* time, an equation speed relative position;
- For the experimentally cooling rate the methodology used is described in Okamoto and Kishitake (1975), where it is obtained from the Finite Difference numerical method which is based on contained T_L reference in the cooling curves for each position of the thermocouples referring to metal interface /mold. Experimental rate is calculated by the module of the ratio between temperature ranges and time obtained before and after the passage of the T_L for each thermocouple, so that:

$$\dot{T} = \frac{\partial T_{liq}}{\partial t} = \frac{\Delta T}{\Delta t} \tag{2}$$

5. RESULTS AND DISCUSSION

5.1 Solidification Speed

The figure shows the solidification curve with vertical lines delimiting the transit time of the *liquidus isotherm*. This transit time is identified from the *liquidus* temperature of the alloys.

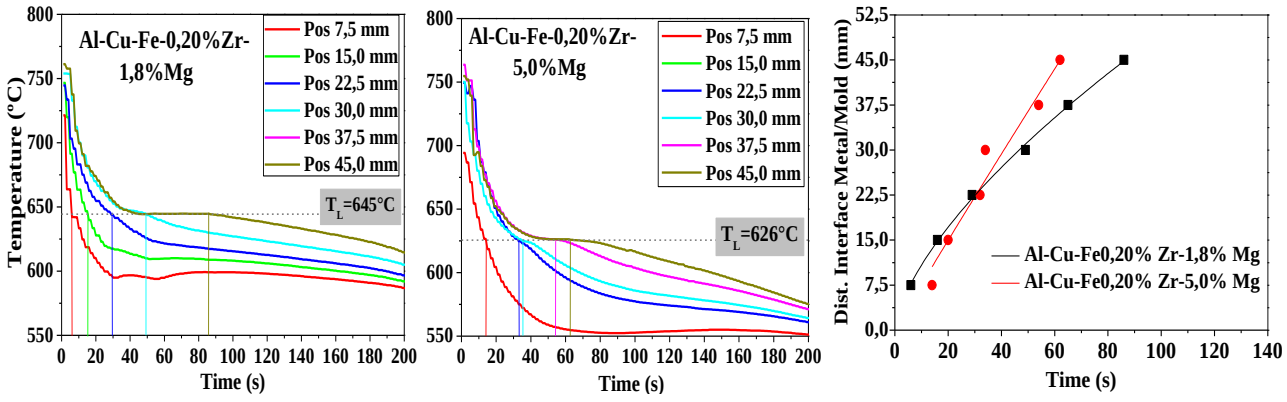

Figure 8. Solidification curves for alloys delimiting the transit time T_L for obtaining the position versus time graph (personal archive, 2016)

Below are shown the graphics solidification speed versus time and location. The blue, black and red lines represent the alloys without the addition, and adding 1,8wt% and 5,0wt% of magnesium respectively:

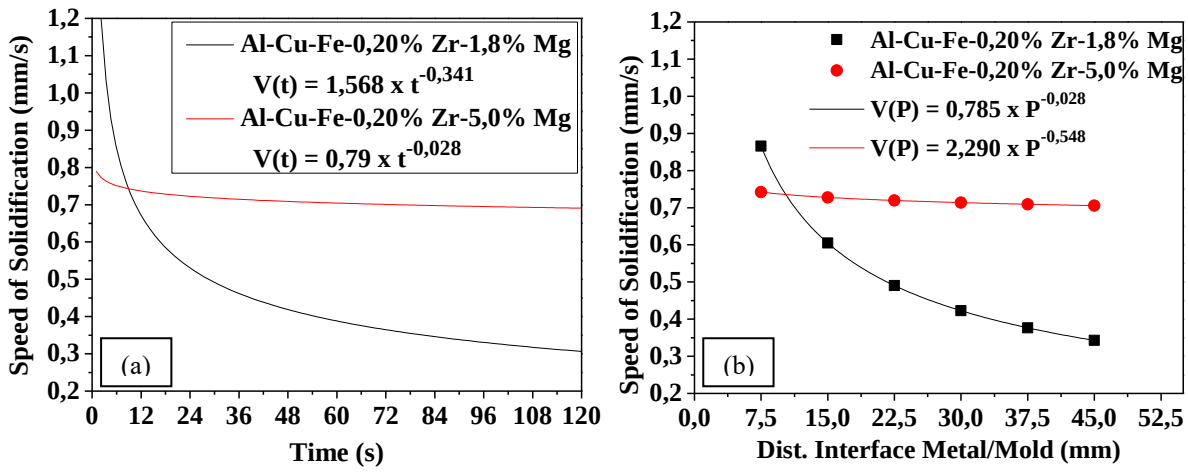

Figure 9. (a) chart speed x time and (b) speed x position (personal archive, 2016)

The table below shows the speed of solidification position values versus time for each alloy:

Table 1. Solidification speeds to each position. Results for alloys with 1,8 and 5,0wt% Mg.

Position (mm)	Al-1,8wt% Mg (mm/s)	Al-5,0wt% Mg (mm/s)
7,5	0,86	0,74
15	0,60	0,73
22,5	0,50	0,72
30	0,42	0,71
37,5	0,38	0,71
45	0,34	0,70

It is noted that although the present alloys nonlinear behavior, it can be seen that the solidification rate in the 5,0wt% Mg alloy has a more homogeneous profile with respect to the other. Despite 1,8wt% Mg alloy having a higher speed in the 7,5 mm position in the other positions speed is lower than the alloy with 5,0wt% Mg, and unlike 5,0wt% Mg alloy where there is a speed almost constant, at 1,8wt% Mg alloy presents a sharp drop in the remaining positions.

5.2 Experimental cooling rate

Table 2 shows the results of the cooling rate calculated from the data obtained experimentally from the solidification curves for each alloy studied and plotted in Figure 10 are the values obtained, besides demonstrating the trend line behavior of the cooling rates.

Table 2. Experimental solidification (or cooling) rate *vesus* distance from the metal mold interface.

Position (mm)	Al-1,8wt% Mg (s)	Al-5,0wt% Mg (s)
7,5	11,3	5,11
15	6,65	4,16
22,5	3,44	3,90
30	2,25	3,67
37,5	2,15	2,55
45	1,36	2,28

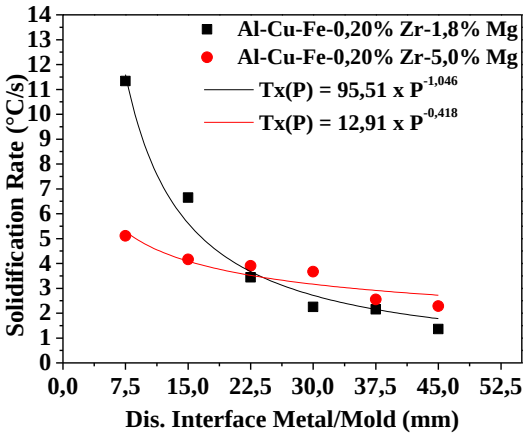

Figure 10. Experimental cooling rate as a function of position (personal archive, 2016)

For cooling rates, 5,0wt% Mg alloy exhibits a more homogeneous behavior to 1,8wt% Mg alloy. The alloy containing 1,8wt% Mg showed the highest cooling rate at the position 7,50 mm and 45,0 mm at the lower rate position.

5.3 Macrostructure of solidification

The macrographs alloys are shown in Figure 11, and Figures "a" and "b" with additions of 1,8% to 5,0%. It can be seen that both macrostructures adding Mg alloys suggests a predominance of equiaxed grains. Can relate to the grain refining of high solute concentration associated with rapid cooling. The macrographs were obtained after use of the reagent Keller surface for 5 seconds.

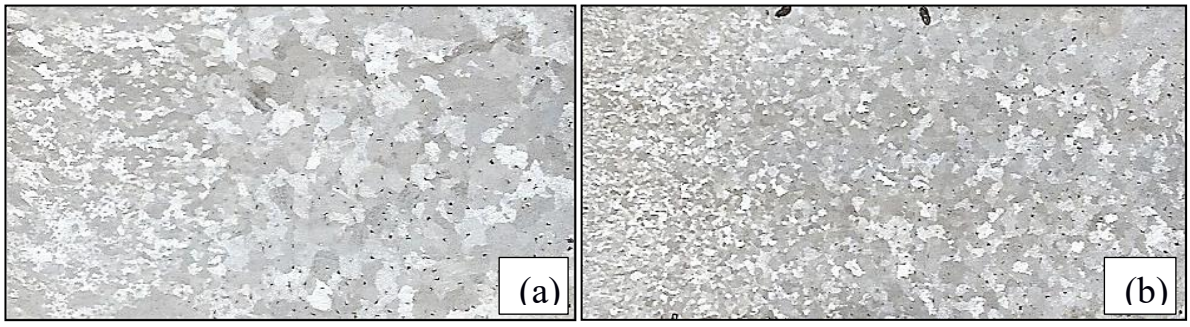

Figure 11. Macrostructures of alloys (a) 1,8wt% Mg and (b) Mg 5,0%, respectively, in real size (personal collection, 2016)

The figure below is the relationship between the cooling rate of the alloy with additions of Mg and their macrostructure.

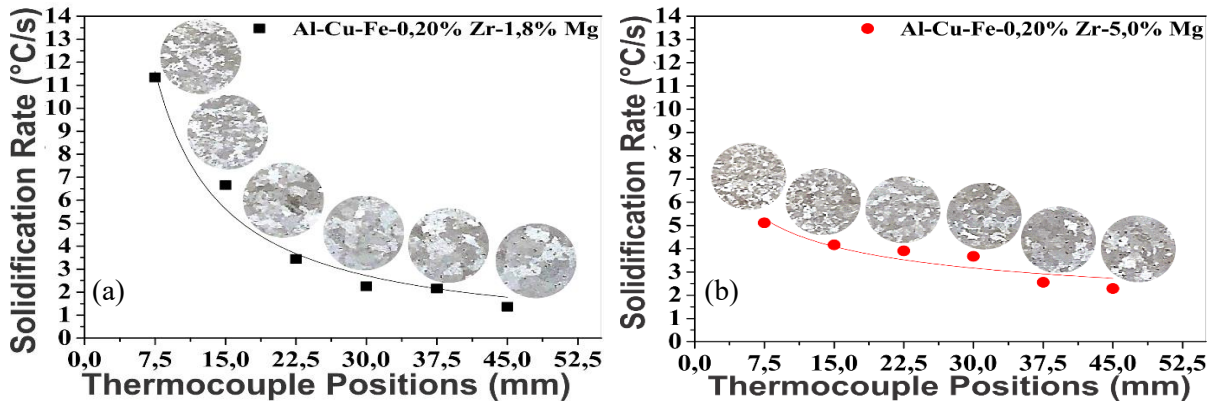

Figure 12. Graphs of solidification rates and macrographs (increase of 10x) for positions of alloys with (a) 1,8wt% Mg and (b) 5,0wt% Mg, respectively (personal collection, 2017)

The two alloys with magnesium addition have a predominantly equiaxed grains throughout the casting region. The alloy has 1,8wt% Mg rate 11,34° C/s (higher in alloys). The macrographs correlated with rates indicate that the addition of magnesium initially increases the cooling rate. In particular, the 1.8wt% Mg alloy showed a sharp decreasing graph. It can be seen that the grain size increases as it distances itself from the metal/mold interface.

The alloy added with 5,0wt% Mg showed a more regular cooling rate compared to other alloys (with a variation in magnitude of 2,83º C/s between the first and last position). The cooling rate of this alloy is more uniform, suggesting that addition of this magnesium content can improve heat transfer in the solidification process.

The results are consistent, there is seen that for Garcia (2001c) "both traditional techniques grain control of control consist of the controlled cooling, i.e., high cooling rates for grain refining, and the addition of nucleating agents".

Besides the increase of the cooling rate and the presence of finer grain observed as the addition of magnesium, zirconium, as described by HANDBOOK OF ALUMINUM (2013d) restricts the size of the grains in the solidification process.

5.4 Chemical compositions

The alloy with 1,8wt% Mg showed a maximum variation in 0,0014% zirconium distribution; less than 0,004% a maximum of 5,0wt% Mg alloy. In general, in both alloys there is a tendency of uniformity in the distribution of zirconium having the same little gap extension across the billet.

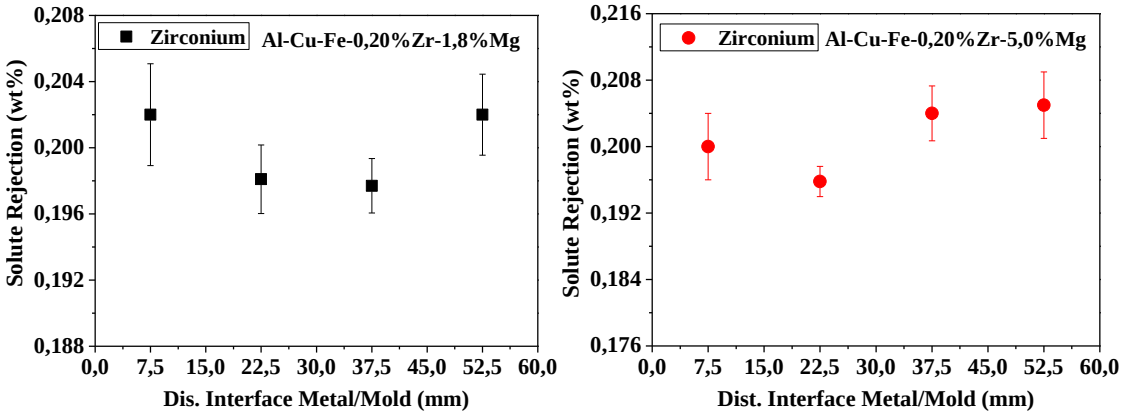

Figure 13. Zirconium chemical compositions of alloys positions without the addition of magnesium, 1,8wt% Mg and 5,0wt% Mg, respectively (personal archive, 2016)

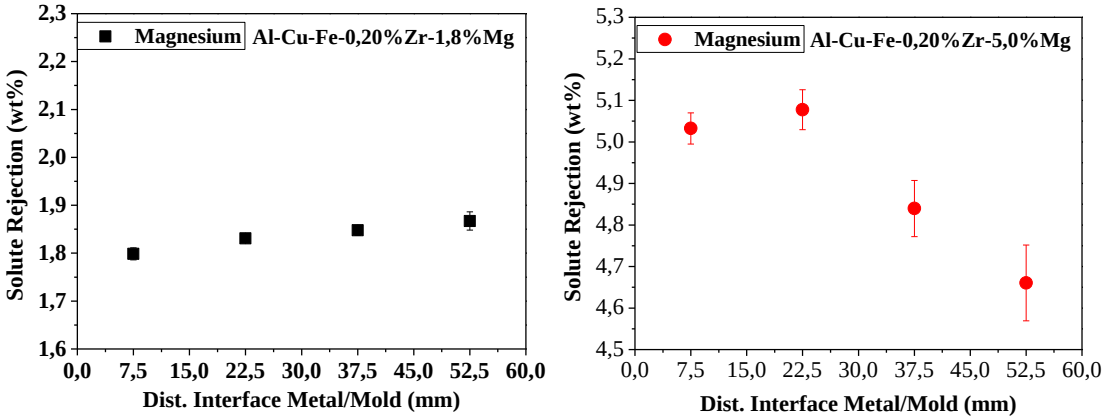

Figure 14. Chemical compositions of positions x magnesium alloys with 1,8wt% Mg and 5,0wt% Mg, respectively (personal collection, 2016)

In both magnesium compositions, profiles are shown opposite as the distance from the metal/mold interface as shown in Figure 14. At 1,8wt% Mg alloy profile is almost linear and increasing. As for concentration of 5,0wt% Mg, despite the slight mismatch concentration in position 22,5 mm, the alloy has a decreasing profile in the extension of the ingot.

5.5 Microhardness

Figure 15 shows the results of Vickers microhardness. The graphs below represent the microhardness of alloys with addition of 1,8% and 5,0% of magnesium, respectively.

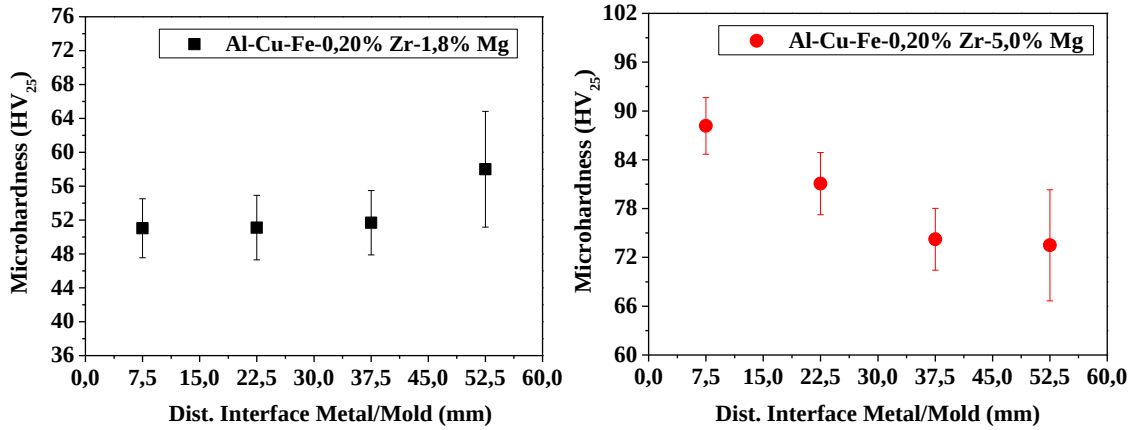

Figure 15. For thermocouples positions microhardness of alloys without the addition of magnesium; 1,8wt% Mg and 5,0wt% Mg, respectively (personal archive, 2016)

Note that the hardness values of the studied alloys follow the behavior of the respective graphics solute rejection. For both alloys with magnesium addition, the hardness appears to follow the magnesium concentration profile according to ingot positions. Another factor is the significant increase of hardness as magnesium addition. The results suggest that magnesium is an element that contributes to the hardening of alloys.

6. CONCLUSIONS

6.1 Assess the macro-structural behavior along the solidification parameters of the alloys

In both alloys by adding Mg equiaxed grains are prevailing. The *equiaxiality* in 5,0wt% Mg alloy begins to be better defined from the position 15,0 mm. In the alloy with 1,8wt% Mg, from 22,5 mm position.

The alloy containing 5,0wt% Mg, with a variation of approximately 0,05 mm/s cooling rate, displays a more homogeneous profile compared to 1,8wt% Mg that, despite a higher speed than 0,85 mm/s 7,50 mm at position suddenly decreases at a decreasing curve up to approximately 0,35 mm/s 45,0 mm position.

Referring to the cooling rate, the alloy with 1,8wt% Mg it is possible to observe a high variation in the cooling rates at each position. The initial position is a peak of 11,34º C/s and the end position 1,36° C/s. In the 5,0wt% Mg alloy, although it also has a decreasing behavior, with maximum 5,41° C/s at the position 7,5 mm and a minimum of 2,08° C/s at the position 45 mm, the variation rate significantly small between each position.

Analyzing the magnesium addition, it is noticed that this possibly increases both the rate, the solidification speed, since the alloy with higher content had increased speed in almost all positions while maintaining higher temperatures for longer.

6.2 To evaluate the distribution of the solute from the metal/mold interface of the alloy as cast

For alloy with addition of 1,8wt% Mg, in general, the concentrations of solutes tend to increase the extent to which distance from the metal / mold interface. In this case, the concentration of zirconium presents a homogeneous profile in relation to the concentrations positions.

The iron and magnesium concentrations in the 5,0wt% Mg alloy exhibit a decreasing character to the extent that metal moves away from the interface. The graph of zirconium concentration homogeneity suggests the extent of the ingot, despite a slight disagreement in 52,5 mm position.

The microhardness of the two alloys with magnesium added followed solute concentration profiles in general. The alloy with 1,8wt% Mg showed a hardness growing character as that metal moves away from the interface. Since the alloy with 5,0wt% Mg showed a decreasing character.

The results show that both alloys with magnesium addition accompany concentration profiles of the respective solutes.

7. ACKNOWLEDGMENTS

Thanks to Professor José Maria do Vale Quaresma for guidance in this work, as well to MSc. Mauro Lobato and Emerson Prazeres contributing indispensably both for the preparation of this work, when to my academic and intellectual progress.

Thanks also to GPEMAT for providing not only all intellectual and structural apparatus, but also the support and personal and professional commitment, especially to you: Clóvis Oliveira, Marcus Wanderley, Marcos Cardoso, Emerson Prazeres, Mauro Lobato, Rafael Assis, Rafael Silva, Fábio Nascimento, Felipe Fernandez, Victor melo, Gregori, Gustavo Neves, Aélcio Santos, Laís Brito and Natália Brum.

8. REFERENCES

ASM International - American Society for Metals, 2003. Aluminum Alloy Production and Materials Manufacturing, American Society for Metals - ASM Handbook. Vol. 2.

CHIAVERINI, V. 1914. Mechanical Technology: Structure and Prospers of Metal Alloys. 2ª ed., vol 1. São Paulo.

DAVIS, J. R. General Introduction. In: ASM SPECIALTY HANDBOOK - Aluminum And Aluminum Alloys. ASM International, Ohio, 1993a. pg. 3-17.

GARCIA, A., 2001a, b, c. Fundamentos e Aplicações", Solidificação, UNICAMP, Campinas. Pg. 22-115.

Kurz, W. e Fisher, D. J., 2003a, b, c, d. Fundamentals of Solidification, Trans Tech Publications, Switzerland, 1992.

MARCEL DEKKER, INC. HANBOOK OF ALUMINUM - Physical Metallurgy and Processes. Vol 1. New York, Basel. pg. 885 – 886, Murat Tiryakioglu and James T. Staley.

Murat, Tiryakioglu and James T. Staley, 2003. Physical Metallurgy and Processes", Hanbook of Aluminum, Vol. 1, New York, Basel, pg 885 – 886, ARCEL DEKKER.

OKAMOTO, T., KISHITAKE, K., 1975. Dendritic Structure In Unidirectionally Solidified Aluminum, Tin, And Zinc Base Binary Alloys. Journal of Crystal Growth, Vol. 29, p. 137-146.

PRAZERES, E., 2014. Study of Thermal Treatment and Modification of the Al-0,05%pCu-[0,24-0,28]%pFe-0,6%pMg alloy with the addition of 0,03wt%Ni, Completion of course work, Belém-PA, pg. 25-26.

QUARESMA, J. M. V., 1999. Correlações Entre Condições de Solidificação, Microestrutura e Resistência Mecânica. Tese de Doutorado, FEM/UNICAMP, CAMPINAS.

RODRIGUES, J. R. P., 2007a, b. Effect of Composition on Thermal and Structural Parameters of Al-Mg Alloys Unidirectionaly Solidified. Doctoral thesis. Pg. 8-12.

9. RESPONSIBILITY NOTICE

The authors Yan Araujo Santos da Campo, Marcus Vinícius Wanderley, Rafael Assis da Silva, Mauro Quaresma Lobato and José Maria do Vale Quaresma are the only responsible for the printed material included in this paper.